



THE PASSIVE TRANSPORT OF NO_x EMISSIONS FROM AIRCRAFT STUDIED WITH A HIERARCHY OF MODELS

PETER F. J. VAN VELTHOVEN,* ROBERT SAUSEN,† COLIN E. JOHNSON,‡
HENNIE KELDER,* INES KÖHLER,† ANNETTE B. KRAUS,§
RADIELA RAMAROSON,¶ FRANZ ROHRER,§ DAVID STEVENSON,||
ASBJØRN STRAND** and WIEL M. F. WAUBEN*

*Royal Netherlands Meteorological Institute, P.O. Box 201, NL 3730 AE De Bilt, The Netherlands;
†Deutsche Forschungsanstalt für Luft- und Raumfahrt, Postfach 1116, D-82230 Oberpfaffenhofen,
Germany; ‡Hadley Centre for Climate Prediction and Research, London Road, Bracknell, RG12 2SY,
U.K.; §Forschungszentrum Jülich GmbH, Institut für Chemie 3, Postfach 1913, D-52425, Jülich, Germany;
¶Office National d'Etudes et de Recherches Aérospatiales, 8 Rue des Vertugadins, F-92190 Meudon,
France; ||Meteorological Office, London Road, Bracknell, RG12 2SY, U.K.; and **NERSC, Edvard
Griegsvel 3A, N-5037 Solheimsviken, Norway

(First received 7 February 1996 and in final form 12 July 1996 Published March 1997)

Abstract – The passive transport of aircraft emissions of nitrogen oxides ($\text{NO}_x = \text{NO} + \text{NO}_2$) has been studied with a hierarchy of models ranging from two-dimensional and three-dimensional chemistry transport models up to three-dimensional models of the general circulation. The sink of NO_x was parameterized by an exponential decay process with a globally constant half-lifetime of 10 days. By performing a simple experiment the importance of the various transport processes has been studied. The three-dimensional models show that the monthly mean volume mixing ratio of NO_x varies by a factor of three in the longitudinal direction and the temporal variability is of the order of 30%. In view of the nonlinearity of the chemical processes leading to ozone formation in the presence of NO_x , this implies that the assessment of the effects of subsonic aircraft emissions of NO_x should be done with three-dimensional models. Vertical redistribution by convection strongly affects the maximum NO_x mixing ratio at cruise altitudes, but due to the limited lifetime of NO_x of the order of ten days the most important contribution to the mixing ratio at a certain level usually stems from emissions around that level. The strong static stability in the stratosphere hampers significant dispersion of the subsonic aircraft emissions above the height where the emissions take place for the lifetimes considered here. Some model deficiencies and biases have been identified and discussed. Examples are the oscillatory signature of NO_x distributions obtained with a spectral advection scheme, the strong diffusion of one of the GCMs into the polar regions, and the too intense interhemispheric exchange of one of the two-dimensional CTMs. For the vertical redistribution of the emissions it may be necessary to include not only updrafts but also downdrafts in the convective parametrization of the transport model. © 1997 Elsevier Science Ltd. All rights reserved.

Key word index: Passive transport, aircraft emissions, nitrogen oxides, models.

1. INTRODUCTION

Air pollution from subsonic aircraft includes many combustion reaction products and unburned fuel components (Prather and Wesoky, 1992; Schumann, 1994). Model simulations indicate that nitrogen oxides ($\text{NO}_x = \text{NO} + \text{NO}_2$) emitted by aircraft contribute significantly to the background concentration of NO_x in the upper troposphere and lowermost stratosphere at northern mid-latitudes (Ehhalt *et al.*, 1992; Kasibhatla, 1993; Wauben *et al.*, 1994; Brasseur *et al.*, 1996). The model predicted enhancement of NO_x by aircraft is roughly consistent with available measurements that indicate characteristic large-scale mixing ratios of 100–500 pptv around the tropopause in the flight corridors and of 10–50 pptv in relatively

unperturbed regions (Drummond *et al.*, 1988; Schlager *et al.*, 1994; Ridley *et al.*, 1994; Emmons *et al.*, 1997). Models predict that the increase of the background NO_x concentration causes a maximum increase in ozone of 3–10% at these heights (Beck *et al.*, 1992; Kasibhatla, 1993; Wauben *et al.*, 1994; Aeronox, 1995; Brasseur *et al.*, 1996; Wauben *et al.*, 1997). At higher altitudes in the middle stratosphere NO_x acts to deplete ozone (Johnston, 1971) and as such was studied in the 1970s when the impacts of supersonic aircraft like Concorde were assessed (e.g. Hidalgo and Crutzen, 1977). It is therefore relevant to study also the possible upward transport of NO_x from subsonic aircraft and to determine the altitude of transition from ozone depletion to ozone production which is not accurately known at present. The radiative

balance of the atmosphere is particularly sensitive to changes in the ozone concentration around the tropopause (Lacis *et al.*, 1990). Assuming an ozone increase in the range of 5–20 ppbv in the North Atlantic Flight Corridor, Fortuin *et al.* (1995) evaluated a radiative forcing in the range 0.03–0.14 W/m² in summer and of 0.01–0.05 W/m² in winter. As well as ozone, the increased concentrations of carbon dioxide, water vapour, and aerosols (Fortuin *et al.*, 1995), and also the formation of contrails (Ponater *et al.*, 1994a), affect the radiative equilibrium of the atmosphere. These radiative changes may in turn change the stratospheric residual circulation (Rind and Loney, 1995) which constitutes a possible feedback on the vertical transport of aircraft pollutants, since the North Atlantic Flight Corridor coincides in latitude with the downward branch of this circulation.

From the above it is clear that a complete assessment of the impact of aircraft emissions of nitrogen oxides upon the atmosphere requires a model that includes the transport of the emitted nitrogen species, extensive ozone chemistry, radiative calculations and possibly a description of feedbacks to the dynamics, i.e. a model of the general circulation of the atmosphere including tropospheric and lower stratospheric chemistry. At present long-term calculations with such a comprehensive model are not yet feasible due to computational limitations. In the European Union project Aeronox (1995) an alternative strategy was chosen to assess the impact of NO_x emissions from subsonic aircraft upon the background concentrations of NO_x and ozone. In Aeronox a hierarchy of models was applied, each model having its own advantages and limitations. Some models included extensive chemistry but rather simplified dynamics, while others contained a realistic description of the general circulation but allowed only for experiments with very much simplified chemistry. In order to integrate the results from the different models and to get an estimate of the model shortcomings, a number of joint experiments were carried out with the models. This paper focuses on an intercomparison of the transport properties of the models used for the assessment of the impact of aircraft emissions of NO_x in the Aeronox project. Seven global models with widely different characteristics were involved in this passive

transport study (see Table 1). The goals were to determine the role of atmospheric transport in the distribution of NO_x emitted by aircraft, and to detect differences in the way the different models handle the transport. Such differences give an indication of the sensitivity of the nitrogen oxide distribution to specific transport processes. The intercomparison of the models with respect to transport also facilitates the interpretation of the differences between the models in simulations including chemistry (Wauben *et al.*, 1994, 1997). The intercomparison includes an analysis of the degree to which the distribution of NO_x is zonally symmetric, and it gives an estimate of its temporal variability due to dynamical processes. These aspects of the current study are of particular interest as the relevant chemistry depends nonlinearly upon the concentrations. Finally, in this study, also the partial contribution of emissions at different altitude ranges to the upper tropospheric NO_x distribution will be investigated. This is important in view of the effectiveness of possible countermeasures like e.g. restrictions with respect to cruise altitude (Sausen *et al.*, 1995).

Three of the models used here (ECHAM3/T21, CTMK and TROPOS) also participated in a recent model intercomparison organized by the World Climate Research Program (WCRP) which aimed mainly at the assessment of the convective parametrizations by simulating a radon-like tracer (Jacob *et al.*, 1996). However, also the dispersion of a very much simplified "aircraft tracer", modelled as a homogeneous emission in the 400–200 hPa column over four line segments, Japan–California, California–New York, Boston–Rome and Rome–Oslo, was studied in the WCRP exercise. It was concluded there that the participating models showed remarkably similar large scale east–west dispersion of the tracer.

The passive transport studies presented here were performed with more realistic sources prescribed according to the Warren Spring Laboratory (WSL) aircraft emission database (McInnes and Walker, 1992). The more elaborate ANCAT (ECAC/ANCAT & EC working group, 1995) and NASA data sets (Wuebbles *et al.*, 1993) were not yet available when most of the model runs were made. For some of the models involved in the intercomparison, simulations with

Table 1. Models involved in this study

Model	Type	Spatial dimension	Mean horizontal resolution (deg)	Mean vertical resolution (km)	No. grid cells or no. parcels
TROPOS	CTM	2D lat-height	7.5	2	288
UIB-2D	CTM	2D lat-height	2.4	1	2,475
CTMK	CTM	3D	5	2.5	51,840
STOCHEM	CTM	3D	1	1.8	10,000
GISS	CTM	3D	9	3.4	7,776
ECHAM3	GCM	3D	8.6 spectral 5.6 semi-Lagr.	2	38,912
EMERAUDE	GCM	3D	5.6	2.6	61,440

emissions from the WSL and the more recent ANCAT data set have been made, but these did not show any qualitative difference regarding the transport of NO_x (Aeronox, 1995). Quantitatively, there are significant differences between the emission databases. The WSL data set gives only a 51% fuel match for 1991/1992, while the ANCAT/EC data set gives a 99% fuel match and the NASA data set gives a 76% fuel match. Also the different emission data sets imply different average NO_x emission indices. For WSL the average emission index was 11.6, for NASA 10.9 and for ANCAT/EC 16.8 g NO₂/kg fuel. If the emissions are scaled up to a 100% fuel match the total NO_x emissions amount to 1.9 Tg (NO₂) yr⁻¹ for WSL and NASA and to 2.8 Tg (NO₂) yr⁻¹ for ANCAT/EC. The experimental set-up of the intercomparison is described in detail in Section 2 and the models involved are briefly described in Section 3. The distributions of the mean NO_x-mixing ratio at three selected heights (200, 500, and 850 hPa) and in a number of vertical north-south cross-sections for January and July have been analysed for most of the participating models. Zonal mean distributions were produced from the results of all models, except GISS.

In the current study, differences in horizontal transport will be exemplarily discussed in terms of the 200 hPa distributions in Section 4. Vertical cross-sections are compared in Section 5, where also differences between two-dimensional and three-dimensional model results are discussed. In Section 6 the

temporal variability on short time scales is analysed, and Section 7 considers interannual variations. Section 8 summarizes the findings from the passive transport studies and offers some discussion.

2. EXPERIMENTAL DESIGN

The NO_x emission database provided by the Warren Spring Laboratory (McInnes and Walker, 1992) was used as a constant source in the simulations of passive transport. The total amount of NO_x emitted by aircraft in 1 yr in this data set is 1.91 Tg (NO₂). This estimate was obtained on the basis of data for a representative week in September 1989. The zonal mean emissions are given in Table 2, where it can be seen that 44% of the emissions take place in the altitude range 10–12 km and that 67% of the emissions occur between 30 and 56 N. Figure 1 shows the geographical distribution of the vertical sum of the aircraft NO_x emissions. Important emission areas are found over the United States, Europe and the Far East and in the air traffic corridors linking them, such as the North Atlantic Flight Corridor between Europe and the United States.

The experimental design attaches a single lifetime to NO_x to enable model intercomparison. The behaviour of NO_x in the atmosphere is more complex with the lifetime being determined by the rate of interconversion between NO_x and NO_y species (such as HNO₃). Thus, in reality, the chemical lifetime of NO_x is expected to be seasonally and spatially variable. To account for the chemical and physical removal of NO_x, e.g. by wet removal of HNO₃, or by dry deposition of HNO₃ at the surface, an exponential decay process with a globally constant half-lifetime of 10 days is applied here. Such a parameterized chemical loss process facilitates the assessment of the differences in transport between the

Table 2. The zonal mean latitude-height distribution of the used aircraft NO_x emission inventory from Warren Spring Laboratory (McInnes and Walker, 1992). The NO_x emissions are given in 10⁶ kg NO₂

Latitude	Height						Sum
	0–2 km	2–4 km	4–6 km	6–8 km	8–10 km	10–12 km	
90–66.4 N	0.659	0.269	0.204	0.168	0.135	13.818	15.253
66.4–56.4 N	10.850	4.697	4.401	4.248	5.152	48.898	78.247
56.4–48.5 N	44.095	19.259	18.921	18.578	22.330	143.197	266.381
48.5–41.8 N	51.441	22.567	21.247	20.626	26.405	133.822	276.107
41.8–35.7 N	93.947	40.594	39.147	38.583	56.043	162.682	430.995
35.7–30.0 N	73.815	30.254	29.509	28.780	37.888	106.659	306.905
30.0–24.6 N	27.154	11.504	11.065	10.821	11.905	63.287	135.736
24.6–19.5 N	20.775	9.564	8.926	8.318	11.135	44.858	103.576
19.5–14.5 N	8.479	3.501	3.268	3.168	3.736	26.328	48.480
14.5–9.9 N	10.779	4.190	4.022	3.858	4.519	16.395	43.764
9.9–4.8 N	4.428	1.978	1.865	1.763	2.524	13.524	26.082
4.8–0.0 N	6.765	2.837	2.769	2.725	2.529	10.831	28.455
0.0–4.8 S	3.230	1.390	1.330	1.340	2.535	8.565	18.389
4.8–9.9 S	3.704	1.557	1.491	1.470	1.785	8.827	18.834
9.9–14.5 S	1.483	0.683	0.661	0.661	0.844	8.410	12.743
14.5–19.5 S	2.602	1.034	0.984	0.946	1.459	8.532	15.557
19.5–24.6 S	5.508	2.428	2.396	2.407	2.663	7.646	23.049
24.6–30.0 S	3.392	1.410	1.340	1.328	1.961	7.418	16.848
30.0–35.7 S	6.202	2.625	2.547	2.483	3.833	7.958	25.648
35.7–41.8 S	3.710	1.526	1.473	1.474	2.460	2.544	13.187
41.8–48.5 S	0.749	0.310	0.290	0.286	0.249	0.354	2.238
48.5–56.4 S	0.137	0.057	0.050	0.049	0.044	0.142	0.479
56.4–66.4 S	0.000	0.000	0.000	0.000	0.000	0.095	0.095
66.4–90 S	0.000	0.000	0.000	0.000	0.000	0.000	0.000
Sum	383.904	164.234	157.906	154.080	202.134	844.790	1907.0

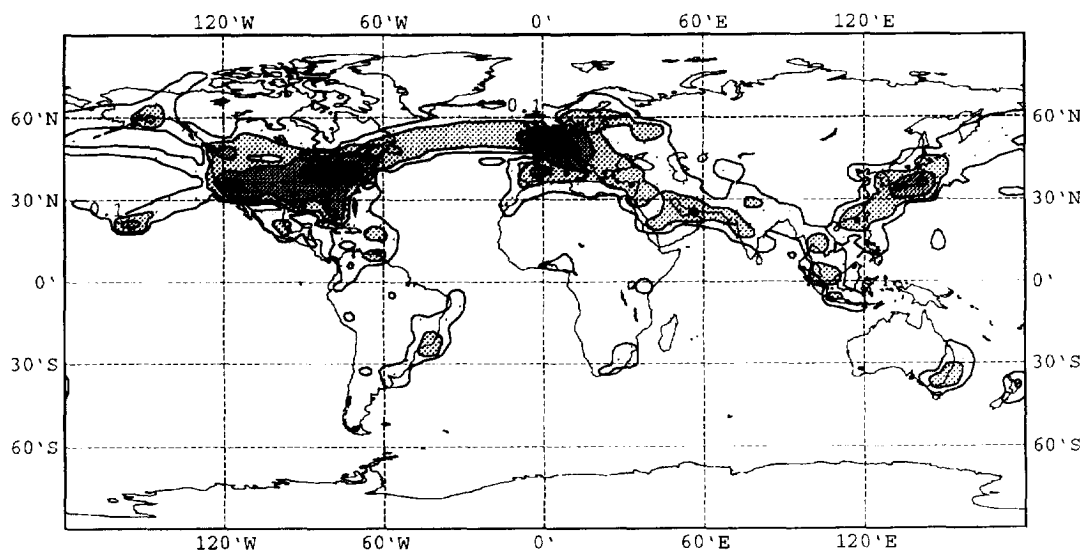


Fig. 1. Geographical distribution of the vertical sum of aircraft NO_x emissions according to the WSL inventory. Contours are drawn at $0.1, 0.3, 1$ and $3 \times 10^{-12} \text{ kg (NO}_2\text{) m}^{-2} \text{ s}^{-1}$. Values between 0.3 and 1 , 1 and 3 , and larger than $3 \times 10^{-12} \text{ kg (NO}_2\text{) m}^{-2} \text{ s}^{-1}$ are indicated by light, medium and heavy shading.

Table 3. Descriptive parameters of the simulations performed with the different models

Model	Spin-up time	Run-time	Simulation mode	Number of months	Archiving interval
TROPOS	1 yr	1 yr	Annual cycle	1	Instantly on 15th of each month
UiB-2D	6 months	12 months	Annual cycle	1	Instantly on 15th of each month
CTMK	3 months	4 yr	Annual cycle	4	12 h
STOCHEM	No	1 month	January/July	1	1 d
GISS	12 months	1 yr	Annual cycle	1	8 h
ECHAM3	6 months	6 months	perpetual	6	12 h
EMERAUDE	No	5 yr	January/July Annual cycle	1	8 h

models. Ten days is a characteristic half-lifetime of NO_x in the upper troposphere, i.e. at the lower end of cruise altitudes of commercial aircraft. NO_x half-lifetimes of 4 and 20 days were also used, but the results are qualitatively similar and will not be discussed extensively here (for details see Sausen and Köhler, 1994).

The models involved constitute a representative sample of the entire set of models used in the Aeronox project for global simulations including chemistry. They are described in Section 3 and summarized in Table 3. The models were run either in the annual cycle mode, i.e. with driving forces undergoing the full annual cycle, or in the perpetual January/July modes, i.e. with the solar constant, the sea-surface temperature, etc., fixed to mid-January and mid-July conditions. The latter technique neglects the seasonal time derivative but it reduces the required computation time for the GCMs drastically and can be applied in order to get a first estimate of certain dynamical or thermodynamical processes which do not critically depend on sea-ice distribution or snow cover. The analysed period was usually preceded by a spin-up period (see Table 3) which was required to achieve a quasi-stationary state independent of the initial conditions. Table 3 also shows the different procedures that were used for calculating monthly averages as a consequence of varying availability of meteorological input data and computer resources.

3. THE MODELS

The hierarchy of models used to perform the passive transport experiments described in Section 2 is described below.

3.1. Three-dimensional general circulation models

The three-dimensional general circulation models (GCMs) ECHAM3/T21 and EMERAUDE, explicitly resolve thermodynamical and dynamical processes at time scales down to about half an hour. The spectral general circulation model ECHAM has been developed jointly by the Meteorologisches Institut der Universität Hamburg and the Max-Planck-Institut für Meteorologie at Hamburg in Germany from a version of the numerical weather prediction model of the European Centre for Medium range Weather Forecasts (ECWMF). The prognostic variables are vorticity, divergence, temperature, (logarithm of) surface pressure, humidity, and cloud water (ice and water phase). A number of different passive tracers can be

transported (Feichter *et al.*, 1991). The model contains parameterizations of radiation, cloud formation and precipitation, convection (including convective tracer transport), and vertical and horizontal diffusion. The model version used in this study is a modification of the operational ECHAM3 T21 model. Humidity, cloud water, and tracers are advected by a semi-Lagrangian scheme (Rasch and Williamson, 1990), which is used in the grid point domain. During an integration time step these variables are never transformed into the spectral domain. A spectral advection scheme is used for the other prognostic variables. The semi-Lagrangian scheme was introduced in order to avoid negative concentrations, which are produced by a spectral advection scheme due to the Gibbs phenomenon. A comprehensive description of ECHAM can be found in Roeckner *et al.* (1992), which also includes a basic climatology of the model. Technical details are given by DKRZ (1992). Ponater *et al.* (1994b) demonstrated that ECHAM in T21 resolution reproduces the observed large scale northern hemispheric variability quite realistically.

EMERAUDE is a spectral meso-strato-tropospheric model (see Cariolle *et al.*, 1990). A package of parameterizations describes the effects of the main physical processes such as the hydrological cycle, radiative transfer, momentum deposition by orographic gravity waves, turbulent vertical diffusion (Louis *et al.*, 1981) and ∇^4 -horizontal diffusion. In EMERAUDE the negative values of tracers with sharp spatial gradients caused by the spectral advection scheme due to the Gibbs phenomenon are corrected by the method proposed by Royer (1986). Tracers do not experience convective transport nor turbulent vertical diffusion.

3.2. Three-dimensional chemistry transport models

The three-dimensional chemistry transport models (3D CTMs) CTMK, GISS and STOCHEM are off-line in the sense that they derive their transport parameters such as winds from precalculated meteorological data, e.g. from a weather forecast model or a GCM. They also resolve dynamical processes rather well when forced by observed or simulated meteorological fields with good temporal resolution and if they include suitable parameterization of subgrid scale processes like convection. However, the dynamics of such models cannot respond to changes in the concentrations of trace gases like ozone. For the present study there is no fundamental difference between the GCM and the 3D CTM simulations since the experimental set-up does not include feedbacks from the trace gas distributions to the dynamics in the GCMs. The meteorological fields in the 3D CTMs have less temporal resolution than in the GCMs due to restrictions in data storage and/or due to the fact that the input fields from the parent model are stored only twice or four times daily, as is the case for ECMWF which is the parent model of CTMK.

The three-dimensional chemistry transport model of the KNMI (CTMK) is adapted from the global tracer transport model TM2 (Heimann, 1995) which in turn is based upon the model of Prather *et al.* (1987). CTMK calculates the horizontal and vertical transport of tracers on the basis of 12-hourly output from the ECMWF weather forecast model (Velders *et al.*, 1994; Van Velthoven and Kelder, 1996). Meteorological analyses of wind, geopotential height, temperature and humidity with a horizontal resolution of 2.5° are integrated/interpolated to the CTMK grid of 4° in latitude and 5° in longitude at time intervals of 12 h. Vertically CTMK has 15 σ levels from the surface up to 10 hPa, with a resolution of about 60 at 250 hPa. The use of observed meteorological data guarantees a realistic description of the actual meteorological situation in CTMK. Advection is calculated with the second-order moments scheme of Prather (1986) whereafter vertical adjustment is applied in order to conserve mass. The subscale convection fluxes are evaluated according to the scheme of Tiedtke (1989) and the parameterization of Louis (1979) is used for the description of boundary-layer diffusion. The CTMK model time step is 1 h and involves four advection time steps in the east-west, 2 in north-south, and 1 in the vertical direction.

The global 3D chemistry transport model GISS was developed by Prather *et al.* (1987). It uses a version with a spatial resolution of $8 \times 10^\circ$ (latitude \times longitude), a vertical resolution of nine sigma layers from the surface up to 10 hPa, and a temporal resolution of 8 h for the transport. One year of transport parameters, temperature, and pressure as calculated with the GISS-GCM (Hansen *et al.*, 1983) serves as driving forces. As in CTMK the tracers are transported according to the second-order moments method of Prather (1986) which improves the effective spatial resolution by more than a factor of 2. Unlike CTMK the convective transport of tracers is described by a non-local convection scheme. Horizontal diffusion of tracers is also included. The U.K. Meteorological Office Lagrangian tropospheric transport and chemistry model STOCHEM (Stochastic transport and atmospheric chemistry model) combines a Lagrangian transport scheme with a chemistry box model. It is a model that was still under development while these runs were made. A Lagrangian transport scheme was chosen to allow the the integration of a detailed NMHC chemical scheme. The basic transport is provided by the movement of constant mass cells through the action of winds provided from a simulation with the UKMO operational model (Cullen, 1993) over the period 1993-94. In principle, the model could be closely coupled to the GCM so that winds would be provided at frequent intervals; however, here the statistical distribution of the wind components has been sampled in the manner of Taylor (1989). The archived data are available with a resolution of 1.25° of longitude and 0.83° of latitude, with nine unevenly spaced intervals on a hybrid grid

from the surface to around 100 hPa. The advection scheme follows that of Walton *et al.* (1988), though no acceleration terms have been applied. The winds were archived for use as mean and standard deviations for each 18 day period. Linear interpolation is used to determine the actual wind components used at the position of each Lagrangian cell. An Eulerian grid has also been incorporated into the model to allow the calculation of concentrations and to provide emissions. Eulerian concentrations are evaluated by averaging mixing ratios over the cells within each grid volume. The Lagrangian cells in one Eulerian volume are incompletely mixed at each time step. This is an essential component of Lagrangian modelling (Walton *et al.*, 1988) and this inter-parcel exchange prevents the cell concentrations from diverging. The version of STOCHEM used in this study did not yet include a parameterization of convective tracer transport.

3.3. Two-dimensional chemistry transport models

In two-dimensional CTMs one spatial dimension is averaged over. The two-dimensional CTMs used in the present study, TROPOS and UiB 2D, were both latitude–height models, i.e. the longitudinal variability is neglected. These models cannot account for the zonal asymmetry in the NO_x -concentration, which appears to be important in view of the nonlinearity of the chemistry. Nevertheless, this type of model is useful as it allows inclusion of more complex chemistry schemes. Provided their limitations are kept in mind a large number of sensitivity experiments is possible with such models.

TROPOS (Tropospheric chemistry model) is a two-dimensional zonally averaged Eulerian grid model with a domain which extends from the Earth surface to 24 km and from pole to pole. Within this domain the model is divided into 288 equal volume cells, with 24 in the horizontal direction and 12 in the vertical. The model has been described in papers by Hough (1989, 1991). The model transport is based on the scheme of Plumb and Mahlman (1987), who calculated the 2D circulation by assuming a flux gradient relationship and deriving the transport coefficients by inversion of this relationship, given gradients and flux statistics from two tracer experiments with the Geophysical Fluid Dynamics Laboratory (GFDL) general circulation model (Mahlman and Moxim, 1978). The effective 2D transport circulation was defined as a combination of the anti-symmetric part of the transport coefficients tensor and the mean meridional circulation and is as such different from the Lagrangian mean and residual circulations. Hough (1989) describes the implementation of this transport scheme in TROPOS, and also the simulation of inert tracer concentrations.

As in TROPOS, the transport in the University of Bergen (UiB) 2D model (Strand and Hov, 1993) is driven by the circulation derived by Plumb and Mahlman (1987) using the output of the GFDL

GCM. The Plumb and Mahlman data describe the mean advection and eddy diffusion fields in the meridional plane up to 10 hPa for the 12 months of the year. A problem with the original data is that they tend to exaggerate the vertical mixing in the stratosphere (Plumb and Mahlman, 1987). Therefore, the vertical diffusion coefficients in the stratosphere in the UiB model have been reduced to a value of $0.1 \text{ m}^2 \text{ s}^{-1}$. The stratosphere in the UiB model is assumed to be the region above a prescribed tropopause, which is located at an altitude z_{TP} related to latitude β by the function $z_{\text{TP}}(\text{km}) = 12.5 + 2.5 \cos(\beta)$. The UiB model uses a horizontal resolution of 75 equally spaced latitude points from pole to pole and a vertical resolution of 33 equally spaced pressure levels from 1000 to 10 hPa. The mass conserving and positive-definite numerical scheme (Bott, 1989) used to solve the transport equations creates only small numerical diffusion (Strand and Hov, 1993). The vertical transport in global 2D models is traditionally parameterized as an eddy diffusion process in addition to the advective transport, but the eddy diffusion parameterization is only valid if the lifetime of the tracer studied is long compared to the timescales at which more or less random motions such as convection and frontal circulation occur, which is not the case for tropospheric ozone or NO_x . In UiB 2D these rapid vertical processes are therefore parameterized by a statistical approach following Langner *et al.* (1990) and Strand and Hov (1993). Since both the mass fluxes and the detrainment profiles are rather uncertain (Strand and Hov, 1994), the parameterization can provide only a qualitative description of rapid vertical transport processes. This is, however, also true for the convective parameterizations in some of the 3D CTMs such as CTMK, where the convective fluxes have to be recalculated from available archived ECMWF parameters because the convective fluxes themselves are not archived by ECMWF.

4. HORIZONTAL TRANSPORT RESULTS

The effect of horizontal transport on the distribution of NO_x can be investigated using the distribution of its volume mixing ratio at the 200 hPa pressure level (approximately 12 km). This level is in the range of main cruise altitudes and close to the tropopause at mid-latitudes. Figure 2 compares the mean January mixing ratio for a number of models.

The main part of the NO_x emissions is found to stay in the Northern Hemisphere within a zonally oriented structure extending from the U.S.A. across the North Atlantic to Siberia. Starting from the geographical distribution of the aircraft emissions (see Fig. 1) this structure arises from eastward transport by the mean wind and from meridional dispersion due to the activity of transient eddies, especially extratropical cyclones. The maximum perturbations found by the models are in broad agreement with measurements

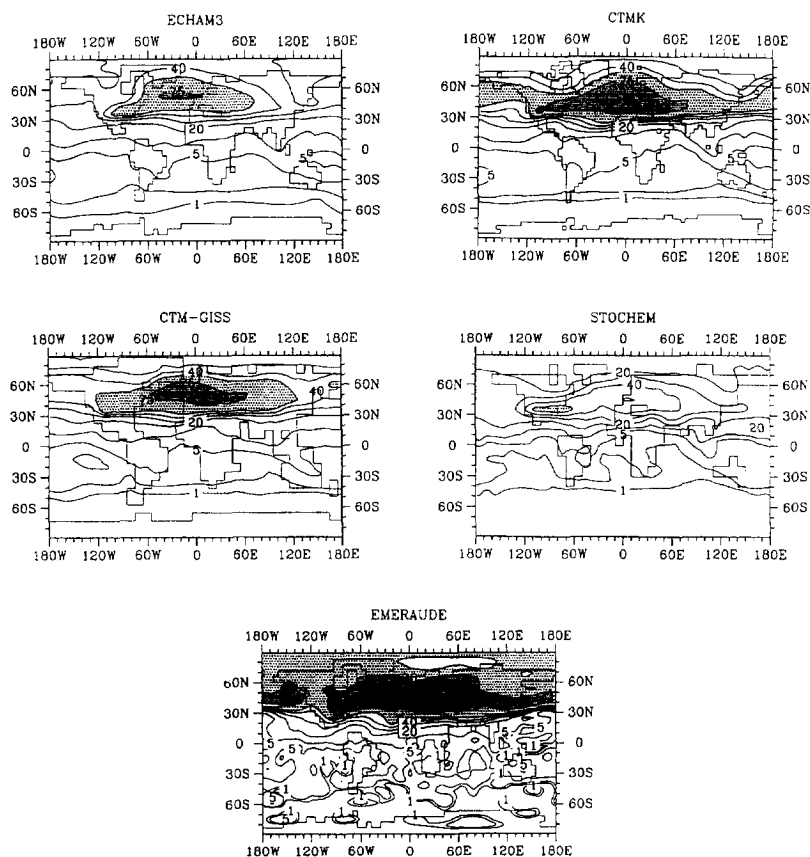


Fig. 2. Mean NO_x volume mixing ratio at 200 hPa for January from ECHAM3, CTMK, GISS, STOCHEM, and EMERAUDE. Contours are drawn at 1, 2, 5, 10, 20, 30, 40, 50, 75, and 100 pptv. Values in the intervals 50–75, 75–100, and larger than 100 pptv are indicated by light, medium, and heavy shading. The land-sea-masks indicate the horizontal resolution of the individual models.

that indicate typical large-scale mixing ratios of NO_x of 100–500 pptv (Emmons *et al.*, 1997), taking into account that 30–60% of the NO_x found in the flight corridor is estimated to be due to aircraft (Wauben *et al.*, 1994; Aeronox, 1995). The geographical distributions from the different models are remarkably similar, apart from EMERAUDE (no convective mixing). In particular, note the resemblance of the 5 and 10 pptv contours in the equatorial region. These show that in all models the interhemispheric exchange is rather slow, as is expected for short-lived gases.

Nevertheless, there are some differences: The gradients in the NO_x concentration north and south of the main corridor are weaker in ECHAM3, EMERAUDE, and STOCHEM than in the other models. The maximum mixing ratio in the flight corridor is somewhat smaller in ECHAM3 than in CTMK and GISS. Clearly, NO_x is more dispersed in ECHAM3 than in these other two models, and ECHAM3 appears to overestimate the meridional transport in January relative to the other models. A similar result was found in a recent intercomparison of radon simulations (Jacob *et al.*, 1996). In the case of STOCHEM

the total amount of NO_x at the 200 hPa level is smaller than for all the other models. The low values are a consequence of the coarse vertical resolution used by STOCHEM so that the initial dilution of the emissions is spread over a thicker layer. The uppermost Eulerian grid cells of STOCHEM extend from 200 to the top of the model at 100 hPa. The vertical resolution of the STOCHEM results was also artificially reduced when the concentrations were transferred from Lagrangian cells to the Eulerian grid. For EMERAUDE the maximum is higher than in all other models, and spurious structures appear in the Southern Hemisphere. The latter are a consequence of the spectral advection scheme that was used in EMERAUDE. Because EMERAUDE does not simulate the convective transport of tracers, the maximum is larger than for models with convective tracer transport.

The characteristic structure of the distributions is not very sensitive to the chosen value for the half-lifetime of 4, 10, and 20 days (Sausen and Köhler, 1994). The reason is that these lifetimes are of the same order of magnitude as the characteristic time of synoptic disturbances (~ 4 d; cf. Heijboer *et al.*, 1996)

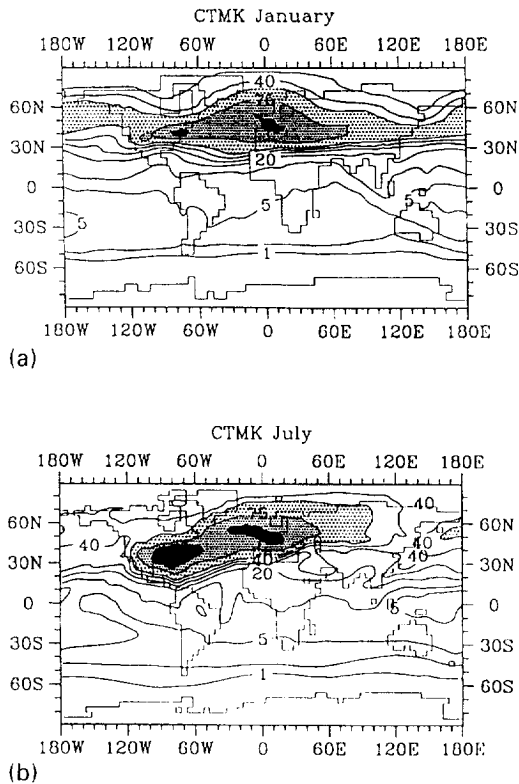


Fig. 3. Mean NO_x volume mixing ratio at 200 hPa for January and July from CTMK. Contours are drawn at 1, 2, 5, 10, 20, 30, 40, 50, 75, and 100 pptv. Values in the intervals 50–75, 75–100, and larger than 100 pptv are indicated by light, medium, and heavy shading.

that are responsible for the meridional mixing. The distribution becomes only slightly more zonally symmetric with increasing lifetime. This emphasizes the necessity of using a three-dimensional model for simulating a realistic NO_x chemistry.

Seasonal variations in effective transport were studied by considering different months. Most of the differences between the models that we found above for January reoccurred in July. Therefore, results from only one model are shown here for July. Figure 3 compares the distributions for January and July from the CTMK model. For CTMK the maximum mixing ratio at 200 hPa is of the order of 125 pptv in July, which is significantly higher than in January (75–100 pptv). The meridional transport of NO_x occurs mainly through mixing by extratropical cyclones. In July the frequency of such transient disturbances is reduced, which explains why the maximum NO_x concentration at cruise altitudes is higher than in January. Furthermore, the distribution is more zonally symmetric in January than in July. In July the maximum is closer to the region of maximum emissions than in January. This is a consequence of the weaker zonal transport in July due to the weaker jet stream in this season.

5. VERTICAL TRANSPORT RESULTS

Figure 4 displays north–south cross-sections at 0° E for January for the three-dimensional models. This longitude was chosen because a maximum in aircraft emissions occurs at this longitude at $45\text{--}55^\circ$ N (over Western Europe). Four of the five displayed three-dimensional models (STOCHEM excepted, because the top of STOCHEM is at 100 hPa.) show a very sharp gradient in the mass mixing ratios in the lower stratosphere just above the height of the emissions. This is due to the high static stability of the stratosphere which hampers vertical transport. The slight vertical excursion of the 1 pptv contour in the GISS result hints towards a somewhat stronger vertical transport in this model, which may be caused numerically by the weaker vertical resolution (see Table 1).

As already noted in Section 4 for the horizontal distributions, the ECHAM3 model shows a smaller maximum and weaker meridional gradients than the other models, as well as larger mixing ratios over the North Pole. One may also note the striking resemblance of the isocontours at 2 and 5 pptv in the equatorial upper troposphere. All models, except STOCHEM, show a tongue-like structure of relatively higher NO_x mixing ratios extending into the Southern Hemisphere in the upper equatorial troposphere. This structure would not be found in measurements since it occurs in the region where lightning sources of NO_x are important (Kasibhatla, 1993; Wauben *et al.*, 1994; Aeronox, 1995). It illustrates, however, the good agreement between the dynamics of the different models. To a certain extent the observed similarity may be explained by the fact that CTMK and GISS use the same advection scheme, while in both CTMK and ECHAM3, the Tiedtke (1989) mass flux scheme for convection is implemented. As CTMK neglects the downdraft from this mass flux scheme, the downward transport of CTMK is weaker than that of ECHAM3 and GISS. In CTMK the downward return flow needed to balance the rapid updrafts in convective cells takes place in the form of slow downward flow in the environment surrounding the clouds instead of partly in vigorous downdrafts. This explains why the maximum at cruise latitudes is somewhat larger in CTMK than in GISS and ECHAM3. The cruise altitude maximum is largest in EMERAUDE which does not include a parametrization of convective transport of tracers at all. STOCHEM also had no convective parametrization in these simulations, but due to the coarse vertical resolution used for emissions input and sampling the results, it produces a smoother distribution than the other models. Finally, it may be noted that the wavy structure of the field of the NO_x mixing ratio in EMERAUDE appears to be a consequence of the spectral advection scheme applied in this model.

Figure 5 compares the zonal mean distribution from the three-dimensional models with the same quantity from the two-dimensional models TROPOS

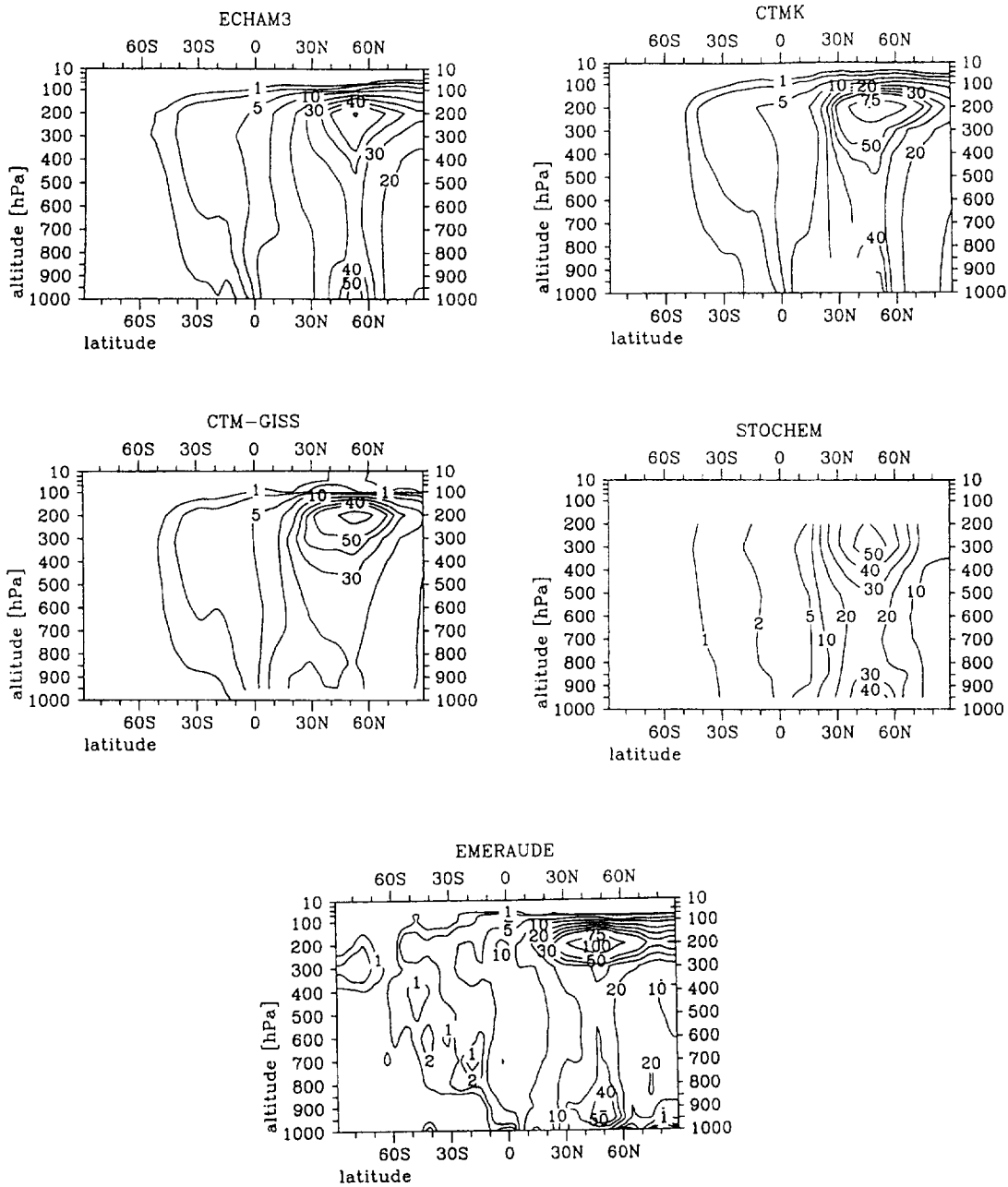


Fig. 4. Latitude–height cross-section at 0° E of the mean NO_x volume mixing ratio for January from ECHAM3, CTMK, GISS, STOCHEM, and EMERAUDE. Contours are drawn at 1, 2, 5, 10, 20, 30, 40, 50, 75, and 100 pptv.

and UiB for January. Figure 6 displays the analogous result for July. The maximum NO_x mixing ratios for January and July are largest in TROPOS and EMERAUDE (more than 75 pptv), which do not simulate the convective transport of tracer. The second highest January mixing ratios are found in UiB (almost 75 pptv) and CTMK (about 60 pptv). In July these models show a small decrease in maximum mixing ratio with respect to January with maxima between 40 and 60 pptv. In contrast, the maximum in

the zonal mean volume mixing ratio in ECHAM3 shows an opposite seasonal behaviour, i.e. in between 40 and 50 pptv in January and more than 50 pptv in July. This could be a consequence of the fact that ECHAM3 appears to overestimate the meridional transport during January. TROPOS hardly shows any seasonal variation. STOCHEM exhibits the same seasonal behaviour as ECHAM3 with a smaller maximum in January. We conclude that the value of the maximum at cruise altitudes is quite sensitive to

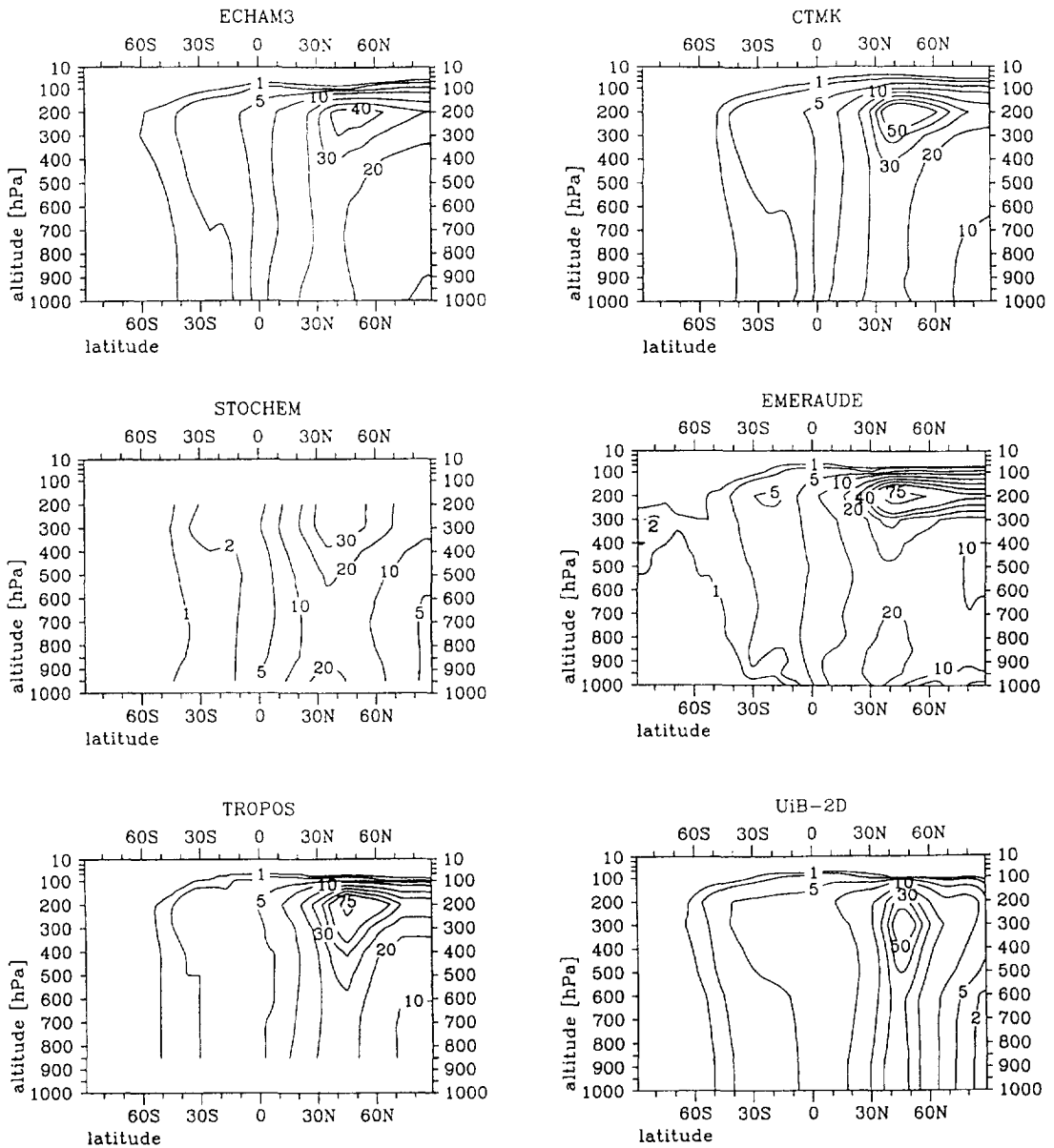


Fig. 5. Latitude-height cross-section of the January zonal mean NO_x mixing ratio from ECHAM3, CTMK, STOCHEM, EMERAUDE, TROPOS, and UiB. Contours are drawn at 1, 2, 5, 10, 20, 30, 40, 50, and 75 pptv.

model formulation, and that it is particularly sensitive to the amount of diffusion and convection, as well as the model resolution.

A secondary maximum in the zonal mean mixing ratio is found at mid-latitudes just above ground level in some of the models. This maximum is partly due to local sources, but its strength and the lower tropospheric mixing ratios in general depends upon the amount of vertical transport by convection. In January this maximum amounts to about 25 pptv in ECHAM3, CTMK, STOCHEM, and TROPOS and to more than 30 pptv in UiB. For EMERAUDE the zonal mean NO_x mixing ratio in the lower and

mid-troposphere is less than 25 pptv. In July all models, except EMERAUDE, show an increase in lower tropospheric NO_x relative to January. EMERAUDE and STOCHEM, which do not simulate the convective transport of tracers at all, have the smallest zonal mean NO_x mixing ratios in the lower troposphere below the maximum at cruise altitudes. In ECHAM3 and CTMK the mixing ratio near the ground is more than 30 pptv in July. This is due to the more intense convective activity in July relative to January, which transports nitrogen oxides emitted at cruise altitudes downward (Sausen and Köhler, 1994).

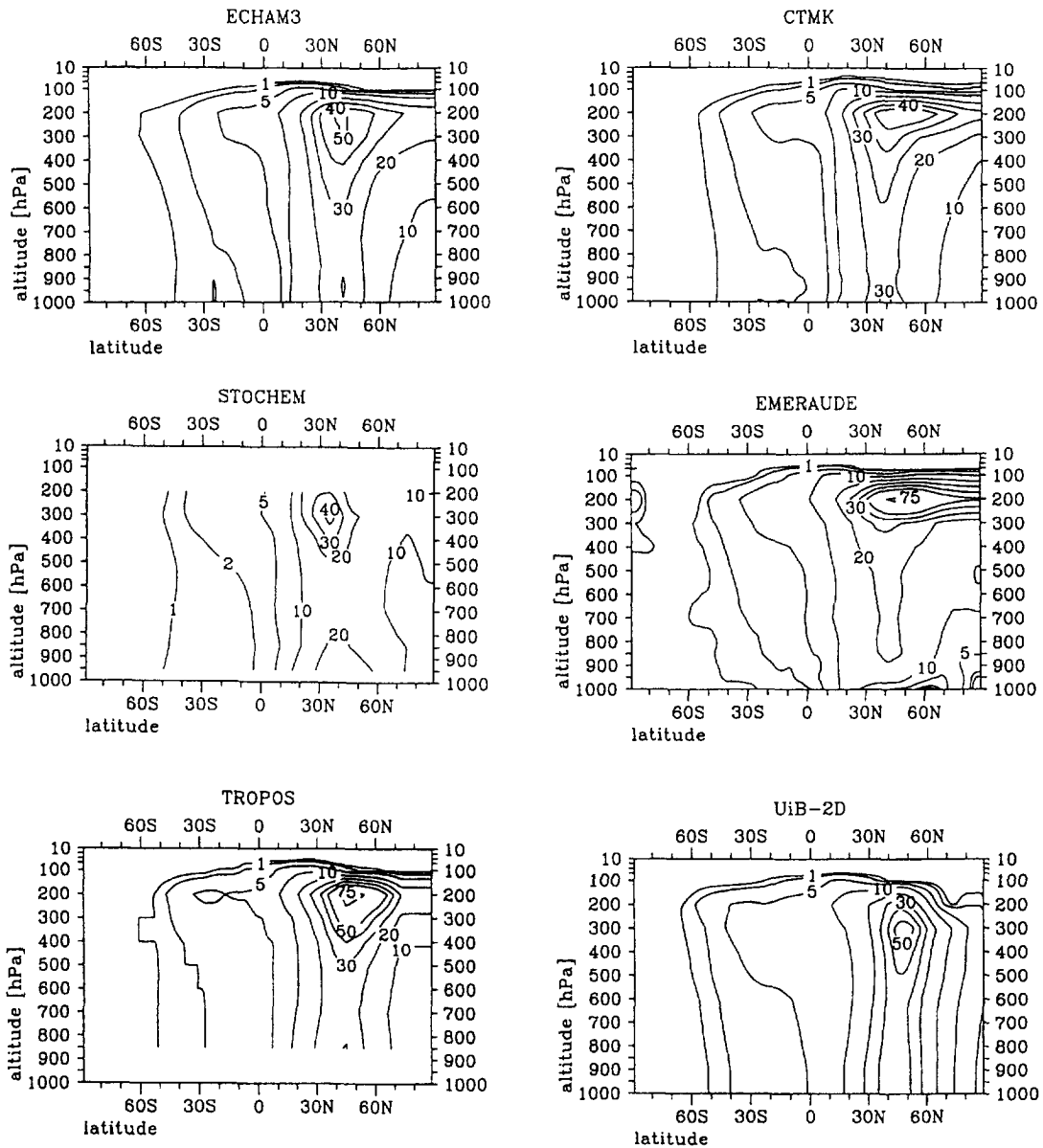


Fig. 6. Latitude–height cross-section of the July zonal mean NO_x mixing ratio from ECHAM3, CTMK, STOCHEM, EMERAUDE, TROPOS, and UiB. Contours are drawn at 1, 2, 5, 10, 20, 30, 40, 50, and 75 pptv.

Let us now consider the tongue of NO_x-rich air in the upper troposphere extending southward over the equator in the three-dimensional models, except STOCHEM (see also Fig. 4). It is reproduced by the two-dimensional models as well, only in the UiB model the 5 pptv contour extends much farther into the upper tropospheric Southern Hemisphere. The 5 pptv contour in UiB almost coincides with the 2 pptv contour for the other models. Hence, the UiB model simulates a larger transport across the equator. Again, the 1 pptv contour line extends farthest into the Southern Hemisphere for ECHAM3. Generally, but especially for July, gradients are somewhat

weaker in STOCHEM than in any other model. This is now considered to be the result of diffusion between Lagrangian cells being too high in the upper layers of STOCHEM. Note further that the gradient in NO_x just above cruise altitudes is similar in all models. In the three-dimensional models (apart from STOCHEM) the vertical transport is limited severely by the large stratospheric static stability. In the UiB model this limitation is artificially introduced by reducing the vertical diffusion coefficient K_{zz} to $0.1 \text{ m}^2 \text{ s}^{-1}$ above the tropopause.

It is expected that organized vertical transport in extratropical cyclones is partly included in the mean

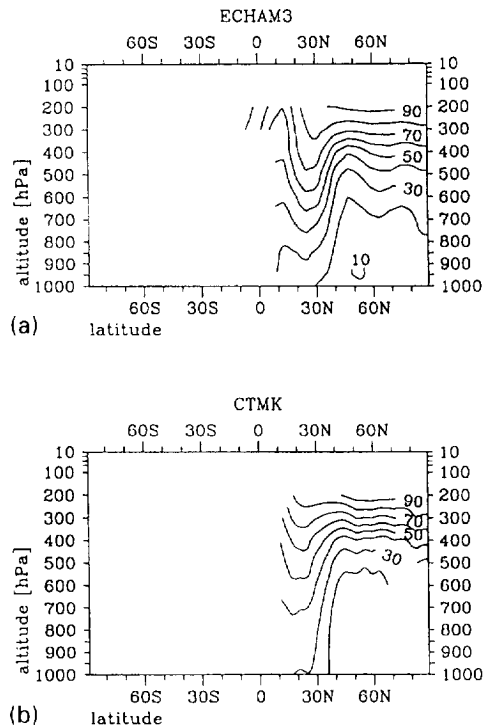


Fig. 7. Latitude–height cross-section at 50°W of the fractional contribution of NO_x emissions at cruise altitude to the total NO_x mixing ratio in July as simulated for ECHAM3 and CTMK. The fractional contribution is displayed only if the total NO_x mixing ratio is larger than 10 pptv. Contours are drawn at intervals of 10%.

vertical motion for the horizontal resolutions of the models used. Convection also contributes to the vertical transport. In order to study the importance of these vertical mixing mechanisms for the NO_x concentrations at various atmospheric heights, the emissions were split into three parts with respect to altitude and the relative contributions of those parts were studied. The boundaries with respect to height were chosen at 365 hPa (approx. 8 km) and 900 hPa (approx. 1 km). The emissions above 365 hPa are due to aircraft at cruise altitudes while the emissions below 900 hPa can be attributed to near-surface emissions in the vicinity of airports (during take-off and landing). The third part of the emissions is due to aircraft flying in the mid-troposphere.

As an example, Fig. 7 shows a vertical cross-section at 50°W of the fractional contribution of the aircraft NO_x emissions at cruise altitudes (above 365 hPa) to the total NO_x mixing ratio as simulated by ECHAM3 and CTMK for July. The longitude of 50°W was chosen because here the traffic within the North Atlantic flight corridor caused a very pronounced signal in the emissions (cf. Sausen and Köhler, 1994, their Fig. 1). The calculations show that July exhibits a stronger vertical mixing than January. The downward mixing of high altitude emissions is evident, but

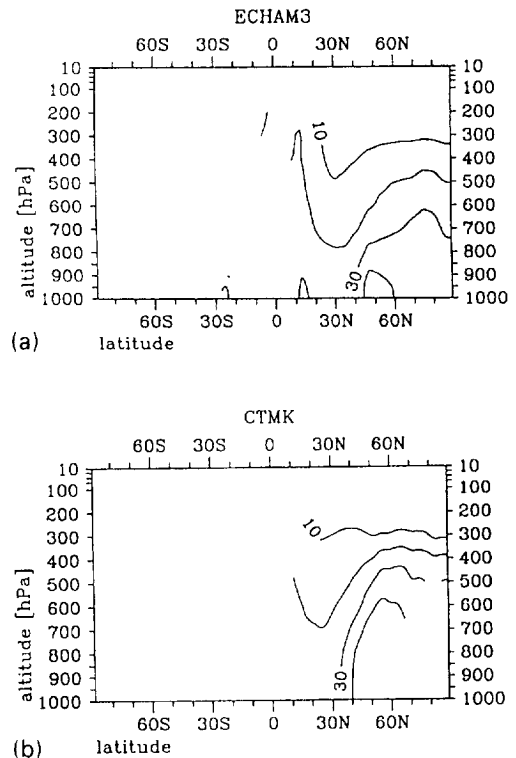


Fig. 8. Latitude–height cross-section at 50°W of the fractional contribution of near surface NO_x emissions from aircraft to the total NO_x mixing ratio in July as simulated for ECHAM3 and CTMK. The fractional contribution is displayed only if the total NO_x mixing ratio is larger than 10 pptv. Contours are drawn at intervals of 10%.

their relative contribution near ground level is small (10–20%). The lifetime of NO_x is probably too small to give a significant contribution, and there are not enough convection events to transport NO_x downward rapidly. We can therefore conclude that most of the NO_x found near the surface was already released at that altitude, i.e. the NO_x found at 50°W at low altitudes arises from near-surface aircraft emissions of the North American continent and was horizontally advected to 50°W . These findings for 50°W remain true for other longitudes (with slight quantitative modifications).

A second experiment is displayed in Fig. 8 where the fractional contribution of the near-surface aircraft emissions to the total NO_x mixing ratio is displayed. Near the maximum of NO_x mixing ratio at the upper levels (cf. Fig. 6) the relative contribution from the sources at lower levels also remains rather small, about 10%. This confirms the result of the previous paragraph. The tropospheric lifetime of NO_x is too small for vertical exchange processes to have a strong impact on the NO_x distribution. It can be concluded that horizontal transport dominates over vertical mixing of aircraft emissions in determining the simulated tropospheric NO_x mixing ratios.

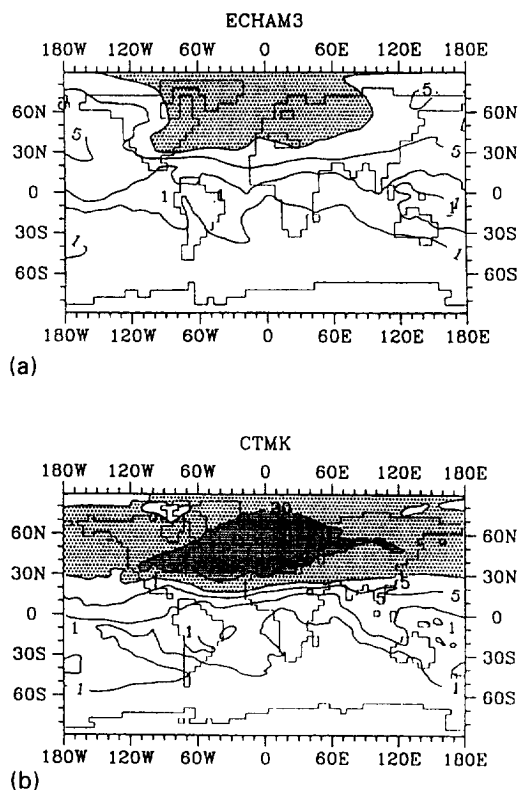


Fig. 9. Standard deviation of the NO_x volume mixing ratio at 200 hPa for January from ECHAM3 and CTMK. Contours are drawn at values of 1, 2, 5, 10, and 20 pptv. Values in the intervals 10–20 pptv, and larger than 20 pptv are indicated by light and medium shading.

6. SHORT-TERM VARIABILITY

In Sections 4 and 5 it was shown that the ECHAM3 and CTMK model are different with respect to the transport to the polar regions and their “diffusiveness”. Here we will show that this can partly be explained by a difference in the underlying description of the weather at synoptic scales. The differences are highlighted when the temporal variability of the NO_x distribution is evaluated. The short-term variability is expressed here by the standard deviation of the 12-hourly values. In the case of CTMK, which was run in the annual cycle mode, the standard deviation of the NO_x mixing ratio was separately calculated for each model month, and subsequently, the long-term mean was computed by averaging the results from the same month of different years (i.e. from all January months). This averaging procedure had to be employed to prevent the storage of excessive amounts of data and because simulations had to be restricted to a time interval of 1 yr. In the case of ECHAM3, which was run in the perpetual January and July modes, the short-term standard deviation was evaluated relative to the long term (6 January or July months) mean by using all 12-hourly data for the month considered. This method produces larger values than the method

used for CTMK, because also the month to month variability contributes significantly to the total variability (cf. Sausen and Köhler, 1994, their Fig. 4). The standard deviation of the geopotential height was calculated according to the “ECHAM3 method” described above for both models. Figure 9 shows the January standard deviations of the volume mixing ratios at 200 hPa for the two models. While the standard deviation for the ECHAM3 nowhere exceeds 20 pptv, it does exceed 25 pptv in the North Atlantic storm track regions for CTMK. Note that the difference between the two models is reduced by the methodology of evaluating the standard deviation. A possible reason for the difference might be that ECHAM3, which evaluates its own weather as a GCM, is inherently limited by its T21 resolution, corresponding to a spatial resolution of roughly 8.6° for dynamical processes, i.e. the model resolution is rather close to the spatial scale of barotropic instability. Consequently, ECHAM3/T21 underestimates the variability of the meteorological fields relative to observations in particular in the North Atlantic sector (Roeckner *et al.*, 1992; Sausen *et al.*, 1993). On the other hand, the dynamics in the CTMK model with its resolution of $4^\circ \times 5^\circ$ is determined by ECMWF analyses, i.e. the observed variability is explicitly introduced into the model. This is demonstrated by Fig. 10 which displays the variability of the 200 hPa geopotential height for January in the ECHAM3 model and in the ECMWF analyses.

The ECMWF analyses show more localized and more intense variability in the storm track regions than ECHAM3. On the other hand, the ECHAM3 model has more uniform regions of high variability extending from mid-latitudes to the polar regions. This could also explain why the transport to the polar regions was stronger and the meridional gradients were smoother in ECHAM3 than in the CTMs (cf. Sections 4 and 5). A definite answer to this question, however, requires further studies, e.g. an inter-comparison of the transient and stationary transports simulated by the various models. The differences in temporal variability, just like the asymmetry of the latitudinal distribution, may have consequences for the chemical perturbations caused by the aircraft emissions, since the chemistry is nonlinear.

7. ANNUAL CYCLE AND INTERANNUAL VARIABILITY

The interannual variability of the NO_x distribution is studied by means of the CTMK simulations, which were forced by the observed meteorology from ECMWF analyses (years 1989–1992). Figure 11 shows Hovmöller diagrams of the zonal and monthly mean mixing ratio of NO_x as a function of latitude and month from January 1989 up to December 1992. The maximum zonal mean NO_x mixing ratios above cruise altitudes (150 hPa) occur in late winter/spring, while at mid-tropospheric levels (500 hPa) they occur

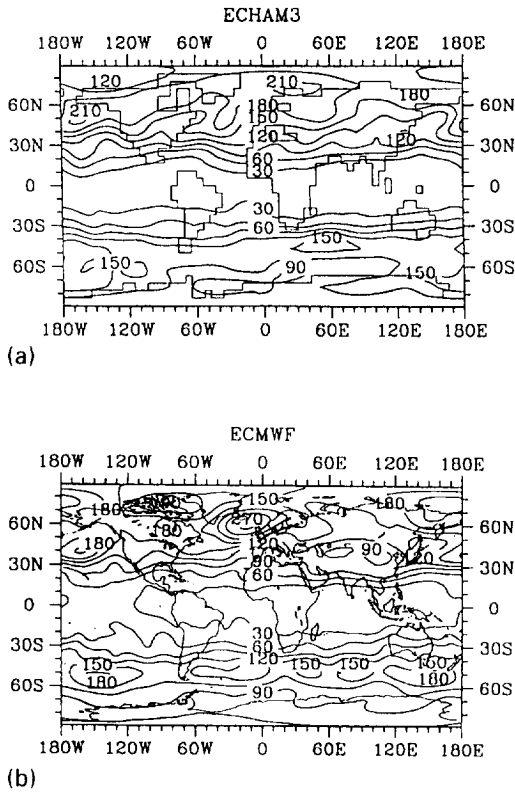


Fig. 10. Standard deviation of the 200 hPa geopotential height for January for the ECHAM3 model and the ECMWF analyses (CTMK). Contours are drawn at intervals of 30 gpm.

in late summer/autumn. The maxima in late winter above cruise altitudes are mainly due to the greater penetration depth of extratropical disturbances into the stratosphere during winter than during summer which promotes vertical transport into the stratosphere. The mid-tropospheric maximum is probably related to the seasonal variation in the height of the

tropopause and the intensity of convection. In winter, the tropopause is in general lower than in summer, so that more of the aircraft emissions occur in the stratosphere (in this study a source constant in time was imposed throughout the year). Less NO_x can, therefore, be transported downward to 500 hPa in winter. In summer, convection is strong and the tropopause is much higher, so that a considerable amount of upper level NO_x can be transported downward to mid-tropospheric altitudes. The seasonal variation of the contours between 50°N and the equator reflects the seasonal displacement of the subtropical jet stream. It is found much farther south in summer than in winter. Generally, the interannual variability is weak over the simulated 4 yr. It is noteworthy that at upper levels (left panel of Fig. 11) there are significant excursions of NO_x -rich air into the polar region in some, but not all, years. This is probably related to year-to-year variations in the strength of the polar vortex in late winter.

8. CONCLUSIONS AND DISCUSSION

The following conclusions concerning the transport properties of the models considered in this intercomparison and concerning the distribution of NO_x emitted from subsonic aircraft can be drawn:

- The distribution of NO_x from aircraft emissions exhibits a strong zonal asymmetry. In the Northern Hemisphere mid-latitudes, the NO_x volume mixing ratios due to aircraft emissions are likely to vary by up to a factor of three longitudinally. This implies that two-dimensional and three-dimensional calculations of ozone formation by NO_x emitted by aircraft may yield rather different results since the chemistry is nonlinear.
- The model results show reasonable agreement between the distributions of NO_x for both January

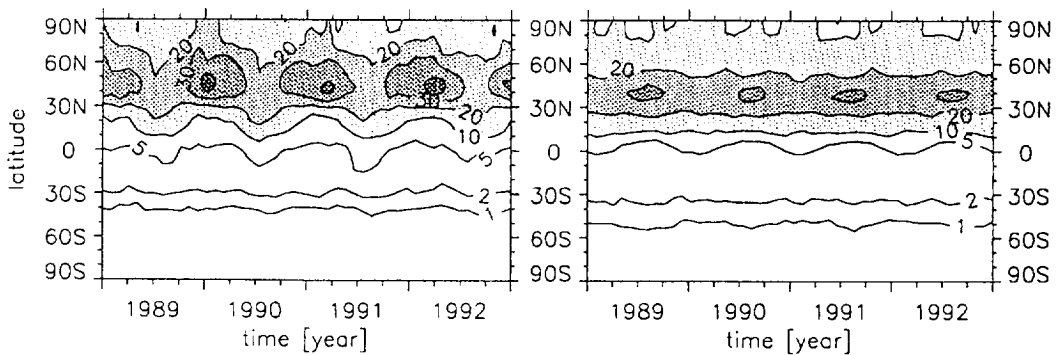


Fig. 11. Zonally and monthly mean volume mixing ratio of NO_x as a function of latitude and month from January 1989 up to December 1992 at 150 hPa (left) and 500 hPa (right) from CTMK. Contours are drawn at 1, 2, 5, 10, 20, and 30 pptv. Values in the intervals 10–20, 20–30, and larger than 30 pptv are indicated by light, medium, and heavy shading.

and July. The calculated NO_x fields exhibit a seasonal variability. In January horizontal transport is more effective than in July, whereas in July vertical transport by convection is stronger than in January. In the course of the year, the zonal mean NO_x mixing ratio at upper levels reaches its maximum values in late winter, while in the middle and lower troposphere maximum values occur in late summer. Note that this was concluded by using a source constant in time throughout the year, and a sink parameterized as an exponential decay process with a temporally and spatially constant lifetime. This need not be true for more realistic lifetimes varying with height, latitude, longitude, season and time of day.

- All models with only one exception show a strong decrease of the NO_x concentration in the stratosphere above the cruising altitudes. Thus, it is likely that, for NO_x lifetimes in the order of tens of days, NO_x emitted by aircraft at cruising altitude does not affect NO_x concentrations in the mid-stratosphere, but is confined to the lower stratosphere.

- All models reveal a weak net interhemispheric flux of the short-lived NO_x-like tracer from aircraft. This implies that aircraft emissions, which mainly occur in the Northern Hemisphere at present, do not play an important role in the tropospheric chemistry of the Southern Hemisphere.

- The temporal variability of the NO_x mixing ratio on synoptic time scales is of the order of 30% of the background mixing ratio in the North Atlantic Flight Corridor. This may again have implications for ozone formation in view of non-linear chemical processes. Models should have sufficient horizontal resolution to include this variability. The temporal variability appears to be less pronounced in the T21 simulations with ECHAM than in the CTMK simulations based on high resolution ECMWF analyses. Further comparisons are necessary to quantify and understand the effect of the temporal variability.

- Excursions of NO_x-rich air into the Arctic region sometimes occur in late winter.

- Vertical exchange processes, both on the resolved scales (e.g. extratropical cyclones) and sub-scale parameterized processes (e.g. convection) give only a minor contribution to the NO_x concentration found at certain altitudes. NO_x which is found close to cruise altitudes was mainly (for more than 80%) released at cruise altitudes.

These conclusions seem to be insensitive to the assumed lifetime of NO_x which was varied between 4 and 20 days. Exchanging the WSL aircraft emission database with the more recent ANCAT database does not significantly influence the conclusions (cf. Aeronox, 1995).

The ECHAM3/T21 model seems somewhat more "diffusive" than some other three-dimensional models, the chemical transport models GISS and CTMK, and the other GCM EMERAUDE. This is because GISS and CTMK use an advection scheme with

a higher effective spatial resolution and EMERAUDE did not use the numerically diffusive semi-Lagrangian scheme as ECHAM did. EMERAUDE suffers from spurious structures in the Southern Hemisphere caused by the Gibbs phenomenon. The results of the STOCHEM did not show a sharp gradient in NO_x in the stratosphere just above cruise altitudes because of a coarse vertical resolution, and diffusivities which have been found to be too high in the version used.

The comparison of the two-dimensional model results UiB and TROPOS led to some interesting conclusions. The models are both modified versions of the model of Plumb and Mahlmann (1987), but UiB had a much better spatial resolution and its dynamics have also been modified to a greater extent. For instance, in UiB the tropopause has been introduced artificially by reducing the vertical diffusion coefficient in the stratosphere. Although this has not been done for the other 2-D model TROPOS, both models were able to represent the strong decrease with height of the NO_x concentration just above the height of the emissions in the lower stratosphere. The introduction of an artificial tropopause as a barrier for vertical transport is therefore of only minor importance for the correct simulation of the NO_x distribution. For tracers with longer lifetimes this would probably be different. The introduction of a convective parameterization in UiB made the simulation of UiB significantly more complete than that of TROPOS which lacks such a parameterization. Finally, the UiB model was shown to have substantially more transport from the Northern into the Southern Hemisphere in the equatorial upper troposphere than any of the other models. The reason for this is as yet unclear.

The models lacking a parameterization of the convective transport of tracers, like EMERAUDE, were shown to have much less vertical transport from cruising altitudes down to the middle and lower troposphere in northern mid-latitudes than the models including such a parameterization.

Acknowledgements—The model intercomparison presented in this paper was funded by the Commission of the European Communities through the project Aeronox under CEC contract: EV5V-CT91-0044. Dr C. Johnson received support from the Department of Transport and the Department of Trade and Industry, London.

REFERENCES

- Aeronox (1995) The impact of NO_x emissions from aircraft upon the atmosphere at flight altitudes 8–15 km. In *Final Report tot CEC. CEC contract EV5V-CT91-0044* (edited by Schumann U.), 471 pp. ISBN-92-826-8281-1. Office for Publications of the European Commission, Brussels.
- Beck J. P., Reeves C. E., De Leeuw F. A. A. M and Penkett S. A. (1992) The effect of air traffic emissions on tropospheric ozone in the Northern Hemisphere. *Atmospheric Environment* **26A**, 17–29.
- Bott A. (1989) A positive definite advection scheme obtained by nonlinear renormalization of the advective fluxes. *Mon. Weath. Rev.* **117**, 1006–1015.

- Brasseur G. P., Müller J.-F. and Granier C. (1996) Atmospheric impact of NO_x emissions by subsonic aircraft: a three-dimensional model study. *J. geophys. Res.* **101**, 1423–1428.
- Cariolle D., Lassere-Bigorry A., Royer J.-F. and Geleyn J.-F. (1990) A GCM simulation of the springtime Antarctic ozone decrease and its impact on midlatitudes. *J. geophys. Res.* **95**, 1883–1898.
- Cullen M. J. P. (1993) The unified forecast/climate model. *Meteor. Mag.* **122**, 81–94.
- DKRZ (1992) The ECHAM3 atmospheric general circulation model. Technical Report No. 6, ISSN 0940-9327, 184 pp., Deutsches Klimarechenzentrum, Hamburg.
- Drummond J. W., Ehhalt D. H. and Volz A. (1988) Measurements of nitric oxide between 67°N and 60°S latitude obtained during STRAT0Z III. *J. geophys. Res.* **93**, 15,381–15,849.
- ECAC/ANCAT & EC working group (1995) A global inventory of aircraft NO_x emissions: A first version (April 1994) prepared for the AERONOX Research project. In *AeronoX* (1995) 129–194.
- Ehhalt D. H., Rohrer F. and Wahner A. (1992) Sources and distribution of NO_x in the upper troposphere at northern mid-latitudes. *J. geophys. Res.* **97**, 3725–3738.
- Emmons L. K., Carroll M. A., Atherton C., Hauglustaine D., Levy II H., Rohrer F., Volz-Thomas A., Gerbig C., Wauben W. M. F., Van Velthoven P. F. J., Bakwin P., Bradshaw J., Sandholm S., Doddridge B., Dickerson R., Honrath R., Hübler G., Jaffe D., Kondo Y., Munger J. W., Ridley B. A. and Torres A. (1997) Climatologies of NO_x and NO_y: a comparison of data and models. *Atmospheric Environment* **31**, 1851–1904.
- Feichter J., Roeckner E., Schlese U., and Windelband M. (1991) Tracer transport in the Hamburg climate model. In *Air Pollution Modeling and its Application VIII* (edited by Dop H. v. and Steyn D. G.), pp. 497–506. Plenum Press, New York.
- Fortuin J. P. F., Van Dorland R., Wauben W. M. F. and Kelder H. (1995) Greenhouse effects of aircraft emissions as calculated with a radiative transfer model. *Ann. Geophys.* **13**, 413–418.
- Hansen J., Russel G., Rind D., Stone P., Lacis A., Lebedeff S., Ruedy R. and Travis L. (1983) Efficient three-dimensional global models for global studies: models I and II. *Mon. Weath. Rev.* **111**, 609–662.
- Heijboer L. C., Kelder H., Saraber M. J. M. and Van Velthoven P. F. J. (1996) An analytical model describing the basic structure and development of mature extratropical cyclones. *Mon. Weath. Rev.* **124**, 571–582.
- Heimann M. (1995) The global atmospheric tracer model TM2. Technical report No. 10, ISSN 0940–9327, Max-Planck-Institut für Meteorologie, Hamburg.
- Hidalgo H. and Crutzen P. J. (1977) The tropospheric and stratospheric composition perturbed by NO_x emissions of high altitude aircraft. *J. geophys. Res.* **82**, 5833–5866.
- Hough A. M. (1989) The development of a two dimensional global tropospheric model. 1. The model transport. *Atmospheric Environment* **23**, 1235–1261.
- Hough A. M. (1991) Development of a two-dimensional global tropospheric model: The model chemistry. *J. geophys. Res.* **96**, 7325–7362.
- Jacob J. J., Prather M. J., Rasch P. J., Feichter J., Köhler I., Kasibhatla P. S., Verver G., Van Velthoven P. F. J., Dignon J. E., Penner J. E., Bergmann D. J., Genthon C., Balkanski Y. J., Ramonet M., Zimmermann P., Beagley S. R., De Grandpré J., Blackshear W. T., Grose W. L., Rotman D. A., Chiba M., Chipperfield M., Stockwell Z., Shia R.-L., Law K., Wild O., Reeves C. E., Brown M. and Yang H. (1996) Intercomparison of global atmospheric transport models using ²²²Rn and other short-lived tracers. *J. geophys. Res.* (submitted)
- Johnston H. S. (1971) Reduction of stratospheric ozone by nitrogen oxide catalysts from supersonic transport exhaust. *Science* **173**, 517–522.
- Kasibhatla P. S. (1993) NO_y from sub-sonic aircraft emissions: A global three-dimensional model study. *Geophys. Res. Lett.* **21**, 1707–1710.
- Köhler I. and Sausen R. (1994) On the global transport of nitrogen oxides emissions from aircraft. In *Impact of Emissions from Aircraft and Spacecraft Upon the Atmosphere*. (edited by Schumann U. and Wurzel D.), pp. 193–198, DLR-Mitteilung 94-06, ISSN 0939-298X, DLR, Cologne.
- Lacis A. A., Wuebles D. J. and Logan J. A. (1990) Radiative forcing of climate by changes in the vertical distribution of ozone. *J. geophys. Res.* **95**, 1971–1998.
- Langner, J., Rodhe H., and Olofsson M. (1990) Parameterization of subgrid scale vertical tracer transport in a global two-dimensional model of the troposphere. *J. geophys. Res.* **95**, 13,691–13,706.
- Louis J. F. (1979) A parametric model of vertical eddy fluxes in the atmosphere. *Boundary-Layer Met.* **17**, 187–202.
- Louis J. F., Tiedtke M. and Geleyn J. F. (1981) A short history of the P. B. L. parametrization at ECMWF. Workshop on Planetary Boundary Layer Parameterization, 25–27 November 1981, pp. 59–80, ECMWF, Reading.
- Mahlman J. D. and Moxim W. J. (1978) Tracer simulation using a global general circulation model: results from a midlatitude instantaneous source experiment. *J. Atmos. Sci.* **35**, 1340–1374.
- McInnes G. and Walker C. T. (1992) The global distribution of aircraft air pollution emissions. Report LR 872 (AP), 54pp., ISBN 0 85624 731 6, Warren Spring Laboratory, Stevenage, Hertfordshire, England.
- Plumb R. A. and Mahlman J. D. (1987) The zonally averaged transport characteristics of the GFDL general circulation/transport model. *J. Atmos. Sci.* **44**, 298–327.
- Ponater M., Brinkop S. and Sausen R. (1994a) A first approach to the simulation of the impact of contrails on climate. In *Impact of Emissions from Aircraft and Spacecraft Upon the Atmosphere* (edited by Schumann U. and Wurzel D.), pp. 436–441. DLR-Mitteilung 94-06, ISSN 0939-298X, DLR, Cologne.
- Ponater M., König W., Sausen R. and Sielmann F. (1994b) Circulation regime fluctuations and their effect on intraseasonal variability in the ECHAM climate model. *Tellus* **46A**, 265–285.
- Prather M. (1986) Numerical advection by conservation of second order moments. *J. geophys. Res.* **91**, 6671–6681.
- Prather M. J. and Wesoky H. L. (1992) The atmospheric effects of stratospheric aircraft: a first program report. NASA Reference Publication 1272, 244 pp.
- Prather M. J., McElroy M. B., Wofsy S. C., Russel G. and Rind D. (1987) Chemistry of the global troposphere: Fluorocarbons as tracers of air motion. *J. geophys. Res.* **92**, 6579–6613.
- Rasch P. J. and Williamson D. L. (1990) On shape preserving interpolation and semi-Lagrangian transport. *SIAM J. Sci. Comput.* **11**, 656–687.
- Ridley B. A., Walega J. G., Dye J. E. and Grahek F. (1994) Distributions of NO, NO_x, NO_y and O₃ to 12 km altitude during the summer monsoon season over New Mexico. *J. geophys. Res.* **99**, 25,519–25,534.
- Rind D. and Lonergan P. (1995) Modeled impacts of stratospheric ozone and water vapor perturbations with implications for high-speed civil transport aircraft. *J. geophys. Res.* **100**, 7381–7396.
- Roeckner E., Arpe K., Bengtsson L., Brinkop S., Dümenil L., Esch M., Kirk E., Lunkeit F., Ponater M., Rockel B., Sausen R., Schlese U., Schubert S. and Windelband M. (1992) Simulation of the present-day climate with the ECHAM model: impact of model physics and resolution. Report No. 93, 171 pp., ISSN 0937-1060, Max-Planck-Institut für Meteorologie, Hamburg.
- Royer J. F. (1986) Correction of negative mixing ratios in spectral model by global horizontal borrowing. *Mon. Weath. Rev.* **114**, 1406–1410.

- Sausen R. and Köhler I. (1994) Simulating the global transport of nitrogen oxides emissions from aircraft. *Ann. Geophys.* **12**, 394–402.
- Sausen R., Voss R. and Ponater M. (1993) Orographic forcing in ECHAM. *Beitr. Phys. Atmos.* **66**, 239–252.
- Sausen R., Nodorp D. and Land Ch. (1995) Towards an optimal flight routing with respect to minimal environmental impact. In *Impact of Emissions from Aircraft and Spacecraft Upon the Atmosphere* (edited by Schumann U. and Wurzel D.), pp. 473–478. DLR-Mitteilung 94-06. ISSN 0939-298X.
- Schlager H., Schulte P., Volkert H., Busen R. and Schumann U. (1994) Observation of enhanced nitric oxide abundances within the North Atlantic Flight Corridor. In *Impact of Emissions from Aircraft and Spacecraft Upon the Atmosphere* (edited by Schumann U. and Wurzel D.), pp. 336–341. DLR-Mitteilung 94-06, ISSN 0939-298X. DLR, Cologne.
- Schumann U. (1994) On the effect of emissions from aircraft engines on the state of the atmosphere. *Ann. Geophys.* **12**, 365–384.
- Strand A. and Hov Ø. (1993) A two-dimensional zonally averaged transport model including convective motions and a new strategy for the numerical solution. *J. geophys. Res.* **98**, 9023–9037.
- Strand A. and Hov Ø. (1994) Two-dimensional global study of the tropospheric ozone production. *J. geophys. Res.* **99**, 22,877–22,895.
- Taylor J. A. (1989) A stochastic Lagrangian atmospheric transport model to determine global CO₂ sources and sinks – a preliminary discussion. *Tellus* **41B**, 272–285.
- Tiedtke M. (1989) A comprehensive mass flux scheme for cumulus parameterization in large scale models. *Mon. Weath. Rev.* **117**, 1779–1800.
- Van Velthoven P. F. J. and Kelder H. (1996) Estimates of stratosphere–troposphere exchange: sensitivity to model formulation and horizontal resolution. *J. geophys. Res.* **101**, 1429–1434.
- Van Velthoven P. F. J., Wauben W. M. F., Kelder H., Köhler I., Sausen R., Rohrer F. and Kraus A. (1994) A comparative study of global 3-D transport of NO_x emitted by aircraft. In *Impact of Emissions from Aircraft and Spacecraft Upon the Atmosphere* (edited by Schumann U. and Wurzel D.), pp. 174–179. DLR-Mitteilung 94-06, ISSN 0939-298X. DLR, Cologne.
- Velders G. J. M., Heijboer L. C. J. and Kelder H. (1994) The simulation of the transport of aircraft emissions by a three-dimensional global model. *Ann. geophys.* **12**, 385–393.
- Walton J. J., MacCracken M. C. and Ghan S. J. (1988) A global-scale Lagrangian trace species model of transport, transformation and removal processes. *J. geophys. Res.* **93**, 8339–8354.
- Wauben W. M. F., Van Velthoven P. F. J. and Kelder H. (1994) Chemistry and transport of NO_x aircraft emissions in a global 3-D chemical transport model. In *Impact of Emissions from Aircraft and Spacecraft Upon the Atmosphere*. (edited by Schumann U. and Wurzel D.), pp. 241–246. DLR-Mitteilung 94-06, ISSN 0939-298X. DLR, Cologne.
- Wauben W. M. F., Van Velthoven P. F. J. and Kelder H. (1997) A 3D chemistry transport model study of changes in atmospheric ozone due to aircraft emissions. *Atmospheric Environment* **31**, 1819–1836.
- Wuebbles D. J., Mandon D., Seals Jr. R. K., Baughcum S. L., Metwally M. and Mortlock A. (1993) Emission Scenarios development: Report of the emission scenarios committee. In *The Atmospheric Effects of Stratospheric Aircraft: A Third Program Report* (edited by Stolarski R. S. and Wesoky H. L.), 413pp., NASA. NASA reference Publication 1313. Washington.